Available online at www.sciencedirect.com
ScienceDirect
Trans. Nonferrous Met. Soc. China 20(2010) 1345−1350
Transactions of Nonferrous Metals Society of China
www.tnmsc.cn

Effects of heat treatment on corrosion behaviors of Mg-3Zn magnesium alloy

LIU Xian-bin(刘贤斌), SHAN Da-yong(单大勇), SONG Ying-wei(宋影伟), HAN En-hou(韩恩厚)

State Key Laboratory for Corrosion and Protection, Institute of Metal Research, Chinese Academy of Sciences, Shenyang 110016, China

Received 23 September 2009; accepted 30 January 2010

Abstract: The effects of two kinds of heat treatments T4 (solution treatment) and T6 (aging treatment) on the corrosion behaviors of Mg-3Zn magnesium alloy were studied by electrochemical measurements and scanning electron microscopy (SEM). It is found that zinc element enriches along grain boundaries to exhibit a network microstructure for both T4- and T6-treated alloy. For T6 treatment, larger MgZn particles form mainly on grain boundary and fine MgZn particles precipitate on matrix. Compared with cast alloy, T4 treatment could decrease the amounts of MgZn particles, and decrease the zinc content of zinc-rich net-segregation. Electrochemical measurements show that T4 treatment increases the corrosion resistance while T6 treatment decreases the corrosion resistance of Mn-3Zn alloy.

Key words: magnesium alloy; Mg-3Zn; electrochemical impedance spectroscopy; heat treatment; precipitates; electrochemistry behaviors; corrosion

1 Introduction

Magnesium and its alloys play an important role in the automotive, aerospace and electronic industries since they have high specific strength and low densities[1−3]. However, most magnesium alloys have poor corrosion resistance in ambient air or aqueous environments due to their electrochemically active state[4]. Meanwhile, oxide film formed on magnesium and its alloys cannot protect its matrix since its Pilling-Bedworth ratio of magnesium oxides (0.79) is less than 1[5]. Recently, for improving the corrosion resistance or mechanical performance, many new kinds of magnesium alloys were developed[6−9]. There were lots of ways to improve the corrosion performance of magnesium alloys, such as conversion film, micro-arc oxidation, alloying and heat treatment.

The effects of heat treatment on the corrosion behaviors of magnesium alloys were different for different alloys. SONG et al[10−12] reported that T4 (solution) treatment weakened barrier effect because it decreased the quantity of β phase in AZ91D and T6 (ageing) treatment strengthened the barrier effect because it increased the quantity of β phase in AZ91D. The barrier effect can work when β phase was finely and continuously distributed along grain boundaries, but the barrier effects depended on the quantity and distribution of β phase. This result is only available for the alloys containing a large number of β phase distributed along grain boundaries. For a small amount of β phase, the effects of heat treatment on the corrosion behaviors are still not clear.

In this study, binary Mg-3Zn magnesium alloy was selected and the effects of two kinds of heat treatments T4 (solution) and T6 (ageing) on the corrosion behaviors of Mg-3Zn magnesium alloy were investigated.

2 Experimental

2.1 Sample preparation

The experimental material used for this investigation was Mg-3Zn cast alloy with composition (mass fraction) of 3% Zn and 97% Mg. T4 treatment was performed on cast specimens at 320 ˚C for 10 h and then quenched into hot water at about 60 ˚C. For T6 treatment, cast sample was treated at 200 ˚C for 16 h after T4 treatment and then cooled in ambient environment. The fluctuation of temperature was controlled within ±2 ˚C.

Specimens were mounted using epoxy resin and only about 1 cm^2 surfaces were exposed. All samples

Foundation item: Project(2007CB613705) supported by the National Basic Research Program of China
Corresponding author: SHAN Da-yong; Tel: +86-24-23893115; Fax: +86-24-23894149; E-mail: dyshan@imr.ac.cn
DOI: 10.1016/S1003-6326(09)60302-2

were polished to 2 000 grit with SiC paper, fine polished using 0.5 μm diamond paste, ultrasonically cleaned in acetone, and dried in cold air.

2.2 Electrochemical measurements tests

The corrosive medium was 0.1 mol/L NaCl solution (analytical reagent). Potentiodynamic polarization experiments were performed using EG&G potentiostat model 273. Three electrode system was used with Mg-3Zn alloy treated by different heat treatments as working electrode, platinum as counter electrode, and saturated calomel electrode SCE (0.242 V vs SHE) as reference electrode. Measurement regions were set from −0.2 to 0.2 V vs open circuit potential. Measurements began from cathodic side with a constant scanning rate of 0.5 mV/s after initial delay of 400 s.

Electrochemical impedance spectroscopy (EIS) measurements were conducted using a model 5210 lock in amplifier coupled with EG&G potentiostat model 273. Scan frequency ranged from 100 kHz to 10 mHz and perturbation amplitude was 5 mV. The initial delay of 600 s was set to obtain a stable testing system by immersing specimens into 0.1 mol/L NaCl solution at open circuit potential. The experimental data were fitted with ZsimWin3.20 software.

The hydrogen evolution volume was measured using gas collection apparatus[13].

2.3 Observations of corrosion morphology

The specimens were immersed in 0.1 mol/L NaCl solution from 1 to 48 h, and then cleaned in acetone and dried in cold air. The morphologies were observed using Phillips XL30 scanning electron microscope equipped with energy dispersive X-ray spectroscope (EDS). The corroded samples were sputtered with carbon for better morphology observation.

3 Results and discussion

3.1 Microstructure of Mg-3Zn alloy

The microstructure of cast Mg-3Zn alloy consisted of primary α-Mg, zinc-rich net-segregation and MgZn phase, as illustrated in Fig.1(a) and Fig.2(a). Zinc element gathered around grain boundaries to form a network structure, and some casting defects were distributed on boundaries. There were some eutectic structures on grain boundaries according to the binary alloy phase diagrams[14] and the solidification mechanism of metal[15]. MgZn particles looked like bright pearls enchased on grain boundaries. The particle signed "*A*" in Fig.2(a) was MgZn phase proven by three reasons. Firstly, the results of EDS point scan was $Mg_{63}Zn_{37}$ in top right corner of Fig.3, but the size of this particle was not larger than 1 μm which was the

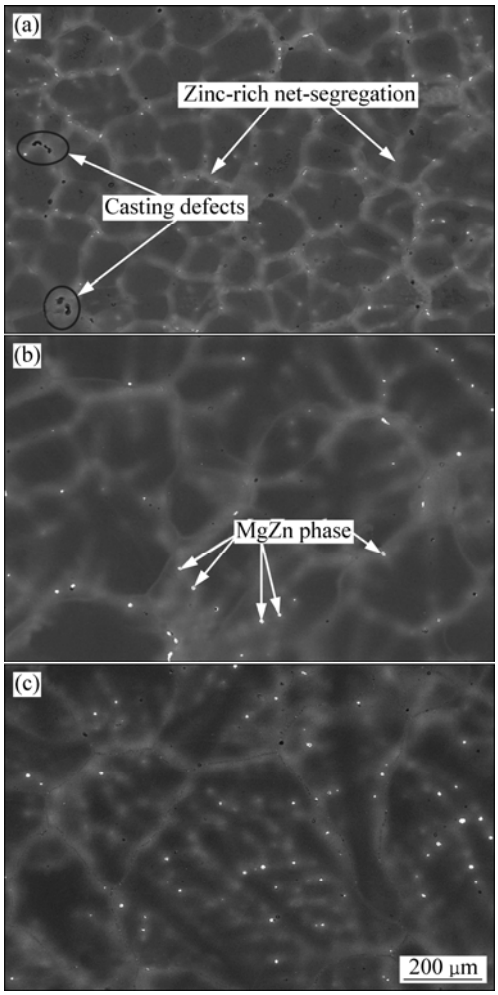

Fig.1 Back-scattered electron images of Mg-3Zn alloys: (a) As-cast; (b) T4-treated; (c) T6-treated

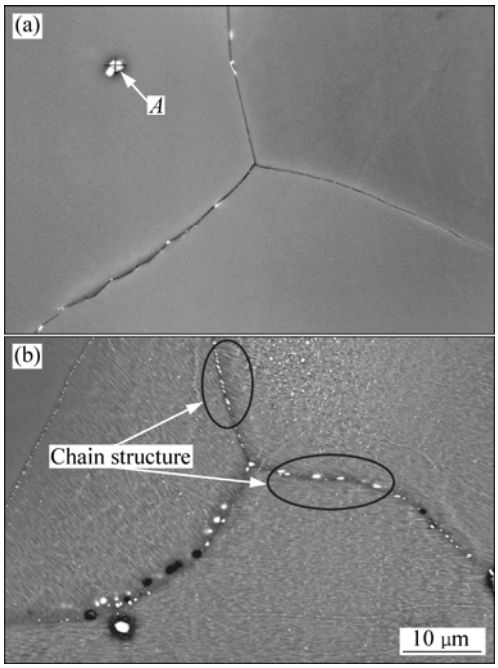

Fig.2 High-magnification SEM images of Mg-3Zn alloys: (a) As-cast; (b) T6-treated

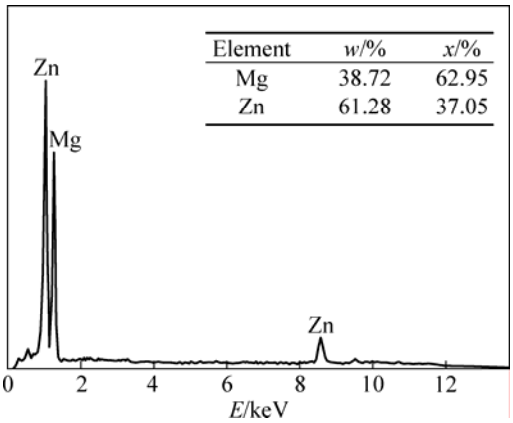

Fig.3 EDS results for point *A* in Fig.2(a)

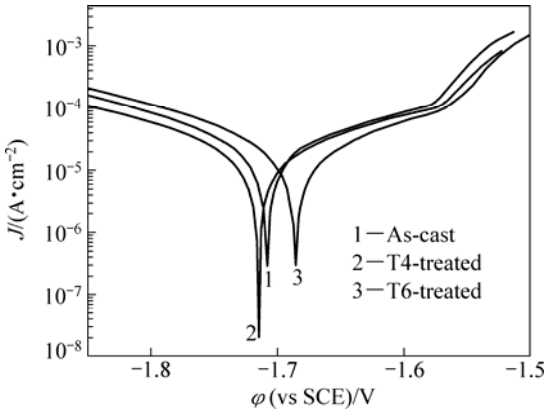

Fig.4 Polarization curves of Mg-3Zn alloy with different heat treatments in 0.1 mol/L NaCl

minimum electron spot size. So, matrix can affect scan result. Secondly, there are only five Mg-Zn intermetallic phases in Mg-Zn alloy, namely $Mg_{51}Zn_{20}$, MgZn, Mg_2Zn_3, $MgZn_2$ and Mg_2Zn_{11}, on account of the binary alloy phase diagrams[14]. Thirdly, this alloy only contained 3% (mass fraction) zinc, so the Mg_2Zn_{11} phase cannot present in solidification structure. It can be said according to analysis above that the particle was MgZn phase. Fine grain was formed because of high solidification rate, and the grain size of cast Mg-3Zn alloy was about 120 μm.

Fig.1(b) shows the microstructure of Mg-3Zn with T4 treatment. The grain size increased to about 240 μm, and the quantity of MgZn particles reduced after T4 treatment. It was found that the distribution of zinc element in T4-treated alloy was more homogeneous than that in cast alloy. In this case, its microstructure was difficult to discern using backscattered electron.

The microstructure of Mg-3Zn with T6 treatment is shown in Fig.1(c) and Fig.2(b). Compared with cast alloy (Fig.2(a)), there were more precipitates formed on grain boundaries and matrix for T6-treated alloy. Some chain structures were visible at grain boundaries, as shown in Fig.2(b). It is found that the grain size was about 300 μm with the increase of holding time, as shown in Fig.1.

3.2 Electrochemical measurements of Mg-3Zn alloys

Fig.4 shows the potentiodynamic curves of Mg-3Zn alloys in 0.1 mol/L NaCl solution after different heat treatments. The curves were fitted using CorrView software in mode of Tafel (traditional). The fitted results are listed in Table 1. Fig.4 and Table 1 indicated that corrosion potential (φ_{corr}) of T4-treated alloy shifted to more negative value compared with that of cast alloy, but the φ_{corr} of T6-treated alloy shifted to more positive value compared with that of cast alloy.

In the case of T4-treated alloy, the quantity of cathodic phase was less than that in cast alloy as shown

Table 1 Fitting results of polarization curves

Alloy	φ_{corr} (vs SCE)/V	J_{corr}/(μA·cm^{-2})	b_a/mV	b_c/mV
As-cast	−1.703	23.8	187	201
T4	−1.715	16.3	207	218
T6	−1.685	18	122	158

in Fig.1 based on two aspects: one was that some of MgZn particles dissolved into matrix, and the other was that solubility of zinc element in matrix was increased, subsequently, the zinc concentration gap between zinc-rich net-segregation structures of boundaries and matrix was less than ever. The more homogeneous structure induced cathodic side of potentiodynamic curves moved left compared with cast alloy and the Tafel slope (b_a and b_c) of T4-treated sample was the largest, as shown in Fig.4 and Table 1.

As for T6-treated alloy, more zinc element was transformed into MgZn phase. As shown in Fig.2(b), there was abundant MgZn particles precipitated in boundaries and matrix. It was obvious that the quantity of MgZn particles in T6-treated alloy was more than that in T4-treated and cast alloy. It was reported that MgZn phase was a strong cathodic phase compared with Mg matrix and the potential difference between them was 0.46 V in 3.5% NaCl solution[16]. Therefore, the increase of cathodic reaction for T6 alloy was due to the presence of more amounts of cathodic phases which induced the accelerated electrochemical dynamic process (b_a and b_c) and decreased the corrosion resistance.

The corrosion behaviors of Mg-3Zn alloys with different heat treatment in 0.1 mol/L NaCl were investigated with EIS measurements at open circuit potential, as shown in Fig.5. The Nyquist diagram for all samples consisted of two loops: a high frequency capacitive loop and a medium frequency capacitive loop. The EIS plots can be equivalent to the circuit shown in Fig.6. High frequency capacitive loop is attributed to the

charge transfer reaction in the electric double layer formed at the interface between metal surface and corrosive medium, which can be described by charge transfer resistance (R_t) and constant phase element (CPE)[17]. The Y_0 and n were two parameters of CPE. The medium frequency capacitive loop is attributed to the mass transport in solid phase, such as the diffusion of ions through the hydroxide or oxide film, which can be described by C_f (a film capacity) and R_f (a film resistance)[18−19]. The equivalent circuit parameters can be calculated with Zsimpwin software and the results are listed in Table 2. The R_t value can disclose the corrosion resistance of alloy in this corrosion medium.

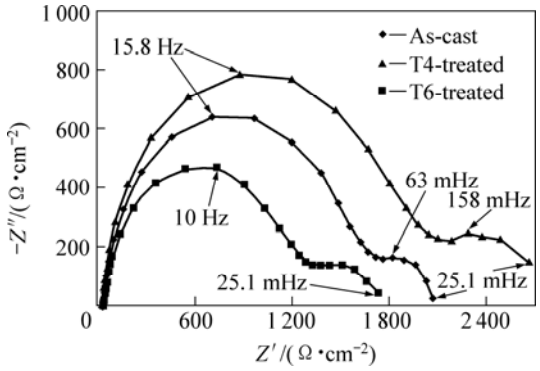

Fig.5 Nyquist diagram for Mg-3Zn alloy with different heat treatments in 0.1 mol/L NaCl solution

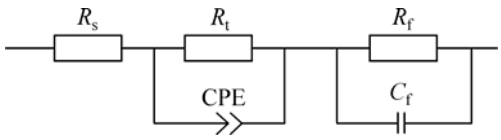

Fig.6 Equivalent circuits of EIS plot for Mg-3Zn alloys with different heat treatments in 0.1 mol/L NaCl solution

Table 2 EIS fitting results for Mg-3Zn alloys with different heat treatments in 0.1 mol/L NaCl solution

Alloy	R_s/(Ω·cm^2)	R_t/(Ω·cm^2)	Y_0/(Ω^{-1}·cm^{-2}·s^{-n})
As-cast	31.45	1 582	11.84×10^{-6}
T4	32.9	1 928	9.29×10^{-6}
T6	34.2	1 217	17.54×10^{-6}
Alloy	n	C_f/(F·cm^{-2})	R_f/(Ω·cm^2)
As-cast	0.910 3	0.002 189	383
T4	0.914 3	0.001 552	580.8
T6	0.892 2	0.002 632	378.8

It was found that T4-treated alloy had the highest charge transfer resistance (R_t) while T6-treated alloy had the lowest. This result indicated that the corrosion resistance of Mg-3Zn alloy could be improved by T4 treatment.

3.3 Immersion tests

Immersion tests were also carried out in a device with the detail of corrosion behavior described in Ref.[13] and H_2 evolution volume was used to characterize the corrosion velocity at room temperature. The testing solution was replaced every 48 h. The ratio of solution volume to specimen area was about 240 mL/cm^2. For cast alloy and T4-treated alloy, there was small difference in H_2 evolution volume in first 3 000 min, as shown in Fig.7. There was an obvious acceleration for all specimens after 3 000 min and the accelerating rate of cast alloy was higher than that of the other two alloys. The conversion relationship of hydrogen evolution volume and the mass loss rate was 1 mL H_2 for 1.084 8 mg Mg[13, 20]. The average mass loss rate of cast, T6- and T4-treated sample was 0.726, 0.657 and 0.612 mg/(cm^2·d), respectively. The corrosion rate of T6-treated sample was higher than that of cast sample in first 4 800 min; however, the average mass loss rate of T6-treated sample was lower than that of cast alloy. The immersion result showed that T4 treatment could improve the corrosion resistance in 0.1 mol/L NaCl solution.

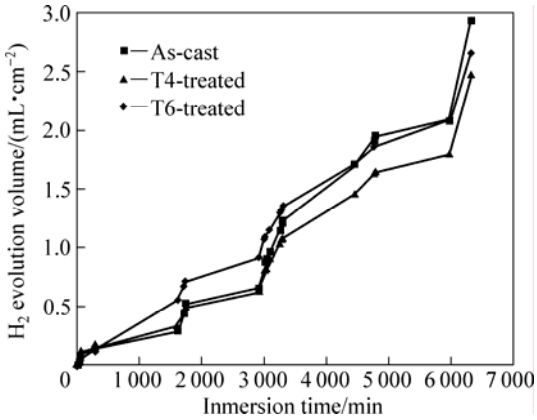

Fig.7 Hydrogen evolution volume for alloys with various heat treatments during immersion in 0.1 mol/L NaCl solution

3.4 Corrosion morphology of Mg-3Zn alloys

It was found that all samples at the same immersion time presented similar morphology. A typical result for T6-treated alloy is shown in Fig.8. For 1 h immersion, there was a thin film formed on sample surface and localized corrosion occurred around MgZn particles, as shown in Fig.8(a). With the increase of immersion time, the MgZn particles peeled off and a hole left, as shown in Fig.8(b). This result indicated that MgZn particles were the cathodic sites which gave rise to the localized corrosion.

4 Transformation of microstructure of heat treated Mg-3Zn alloys

The sketch map is well legible for the effect of heat treatment on the microstructures of Mg-3Zn alloys in Fig.9. The changes of microstructures were embodied on

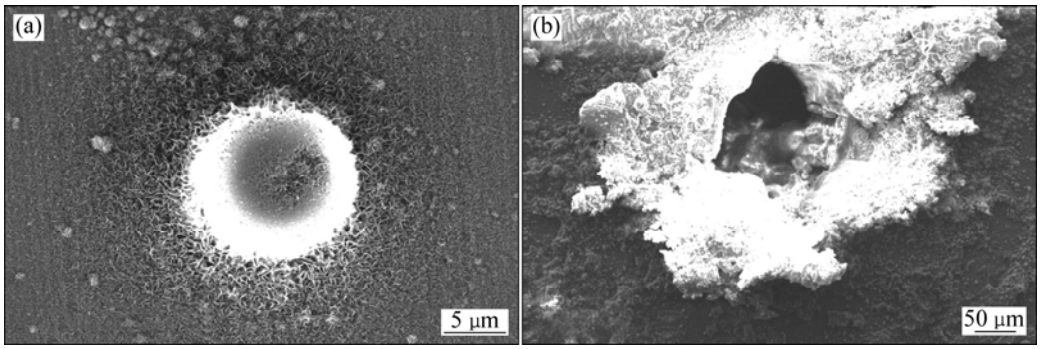

Fig.8 Corrosion morphologies of T6-treated Mg-3Zn alloy in 0.1 mol/L NaCl solution for different time: (a) 1 h; (b) 48 h

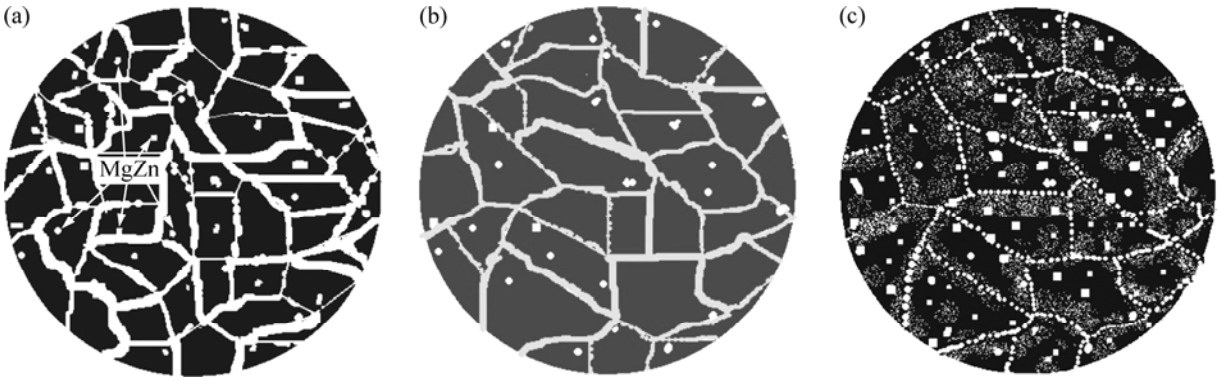

Fig.9 Sketch map for microstructure transformation of Mg-3Zn alloy by heat treatments: (a) Casting; (b) T4; (c) T6

four aspects. First, the grain size was grown form Fig.9(a) to Fig.9(c); second, the maximum quantity of MgZn phase was in T6-treated alloy, and it was the minimum in T4-treated alloy but not all MgZn phases could be dissolved by T4 treatment in Fig.9; third, the network of zinc-rich net-segregation emerged in boundaries, which could not be eliminated by heat treatment carried out in this work. The larger different was the zinc concentration between zinc-rich net-segregation and matrix. The largest range was presented in T6-treated alloy, and the smallest in T4-treated alloy. The last one was that many fine MgZn particles precipitated in matrix and some MgZn particles were grown in boundaries in necklace shape, as shown in Fig.9(c). The corrosion behaviour was a reflection of microstructure.

5 Conclusions

1) Zinc element enriched along grain boundaries to exhibit a network microstructure for both T4- and T6-treated alloys. For T6 treatment, larger MgZn particles formed mainly on grain boundary and fine MgZn particles precipitated on matrix. Compared with cast alloy, T4 treatment could decrease the amounts of MgZn particles, and decrease zinc content of zinc-rich net-segregation.

2) EIS and the immersion experiments showed that T4 treatment increased corrosion resistance while T6 treatment decreased the corrosion resistance of Mn-3Zn alloy. The grain size grew up with the increase of heat treatment time, and the sequence of grain size from fine to coarse was as-cast, T4- and T6-treated alloys.

Acknowledgements

The authors gratefully acknowledge Dr. SHI Bin-qing who provided the Mg-3Zn magnesium alloys. One of the authors, LIU Xian-bin, also wishes to thank professor ZHANG Bo who gave some good ideas and did some modifications for this work.

References

[1] SONG G. Recent progress in corrosion and protection of magnesium alloys [J]. Advanced Engineering Materials, 2005, 7(7): 563−586.

[2] CHENG Y L, QIN T W, WANG H M, ZHANG Z. Comparison of corrosion behaviors of AZ31, AZ91, AM60 and ZK60 magnesium alloys [J]. Transactions of Nonferrous Metals Society of China, 2009, 19(3): 517−524.

[3] FELIU S J, PARDO A, MERINO M C, COY A E, VIEJO F, ARRABAL R. Correlation between the surface chemistry and the atmospheric corrosion of AZ31, AZ80 and AZ91D magnesium alloys [J]. Applied Surface Science, 2009, 255(7): 4102−4108.

[4] LI Z Q, SHAN D Y, CHEN R S, KE W, HAN E H. Corrosion behavior of WE54 magnesium alloy in 3.5%NaCl solution [J]. Transactions of Nonferrous Metals Society of China, 2006, 16: s1806−s1809.

[5] AALLISON E J, COLE G S. Metal-matrix composites in the automotive industry: Opportunities and challenges [J]. JOM, 1993, 45(1): 19−24.

[6] XU D K, LIU L, XU Y B, HAN E H. The effect of precipitates on the mechanical properties of ZK60-Y alloy [J]. Materials Science and Engineering A, 2006, 420(1/2): 322−332.

[7] YANG J, XIAO W, WANG L, WU Y, WANG L, ZHANG H. Influences of Gd on the microstructure and strength of Mg-4.5Zn alloy [J]. Materials Characterization, 2008, 59(11): 1667−1674.

[8] SONG Y W, SHAN D Y, HAN E H. High corrosion resistance of electroless composite plating coatings on AZ91D magnesium alloys [J]. Electrochimica Acta, 2008, 53(5): 2135−2143.

[9] DOBRZANSKI L A, TANSKI T, CZEK L, BRYTAN Z. Structure and properties of magnesium cast alloys [J]. Journal of Materials Processing Technology, 2007, 192/193: 567−574.

[10] SONG G, ATRENS A. Understanding magnesium corrosion-framework for improved alloy performance [J]. Advanced Engineering Materials, 2003, 5(12): 837−858.

[11] SONG G, BOWLES A L, STJOHN D H. Corrosion resistance of aged die cast magnesium alloy AZ91D [J]. Materials Science and Engineering A, 2004, 366(1): 74−86.

[12] SONG G, ATRENS A, DARGUSCH M. Influence of microstructure on the corrosion of diecast AZ91D [J]. Corrosion Science, 1998, 41(2): 249−273.

[13] CHEN J, DONG J, WANG J, HAN E, KE W. Effect of magnesium hydride on the corrosion behavior of an AZ91 magnesium alloy in sodium chloride solution [J]. Corrosion Science, 2008, 50(12): 3610−3614.

[14] MASSALSKI T B, OKAMOTO H, SUBRAMANIAN P R, KACPRZAK L. Binary alloy phase diagrams [M]. The Materials Information Society, 1990.

[15] XU Z, ZHAO L C. Theory on transformation in solid metal [M]. Beijing: Science Press, 2005: 156−157. (in Chinese)

[16] WEI Y H, XU B S. The theory and practice for the corrosion and protect of magnesium alloy [M]. Beijing: Matellurgical Industry Press, 2007: 100. (in Chinese)

[17] MORLIDGE J R, SKELDON P, THOMPSON G E, HABAZAKI H, SHIMIZU K, WOOD G C. Gel formation and the efficiency of anodic film growth on aluminium [J]. Electrochimica Acta, 1999, 44(14): 2423−2435.

[18] GABOVICH A M, VOITENKO A I. Surface tension at the electrolyte solution--metal electrode interface—III. Polyvalent and non-symmetrical electrolytes [J]. Electrochimica Acta, 1990, 35(2): 545−554.

[19] CAO Chu-nan, ZHANG Jian-qing. An introduction to electrochemical impedance spectroscopy [M]. Beijing: Science Press, 2002: 26−30. (in Chinese)

[20] ZHAO M C, LIU M, SONG G, ATRENS A. Influence of the β-phase morphology on the corrosion of the Mg alloy AZ91 [J]. Corrosion Science, 2008, 50(7): 1939−1953.

(Edited by YANG Bing)